

Homogeneous isotropic turbulence: Parameters

Markus Uhlmann

Potsdam Institut für Klimafolgenforschung, D-14412 Potsdam
uhlmann@pik-potsdam.de

(July 2000)

1. Purpose

In the framework of the research project of Klein (1998), detailed time-dependent information of the flow fields in two distinct geometric configurations (homogeneous, isotropic flow; plane channel flow) is needed for the purpose of analyzing the behavior of small-scale instabilities and their influence upon the turbulent energy cascade. Here we describe our first steps towards generating those fields via direct numerical simulation (DNS) in the former case of homogeneous isotropic flow.

2. The equations of motion

For incompressible, constant-density flow, the momentum equations in Cartesian coordinates read:

$$\partial_t u_i - \nu \partial_{jj} u_i = H_i - \partial_i p + f_i \quad , \quad (2.1)$$

where u_i are the components of velocity, ν the viscosity, $H_i = (u_i u_j)_{,j}$ the non-linear term, p the pressure (the density is assumed to be unity for convenience) and f a body force included for the sake of generality. In Fourier space, the system can be written in the following manner:

$$\partial_t \hat{u}_i + \nu k^2 \hat{u}_i = \underbrace{\hat{H}_i \left(\delta_{il} - \frac{k_i k_l}{k^2} \right)}_{\widehat{NL}} + \hat{u}_i h(k) \quad . \quad (2.2)$$

The body force was assumed to be linear in the variable u_i and divergence-free, i.e. $\hat{f}_k = \hat{u}_k h(k)$, where $k_i \hat{u}_i = 0$ (continuity). Note that pressure has been eliminated by substituting the solution of its associated Poisson equation.

The three-dimensional energy spectrum is defined as the spectral energy density of each wavenumber shell (note that $k = \sqrt{k_i k_i}$ is the modulus of the wavenumber vector):

$$E(k) = \sum_{i=1}^3 \hat{u}_i \cdot \hat{u}_i^* \quad , \quad (2.3)$$

the asterisk denoting complex conjugation. The global turbulence intensity is therefore measured by $q^2 = \int_k E(k) dk$ (note also the definition of the r.m.s. one-component velocity $u' = \sqrt{2q^2/3}$). The energy dissipation rate ε is customarily defined in connection with the r.m.s. one-component vorticity ω' as:

$$\varepsilon = \nu \omega'^2 = 2\nu \int_0^\infty k^2 E(k) dk \quad . \quad (2.4)$$

The integral length scale, the Taylor micro-scale and the Kolmogorov scale, used in the following, are defined as:

$$L_{int} = \frac{\pi}{2u'^2} \int_0^\infty k^{-1} E(k) dk \quad (2.5)$$

$$\lambda^2 = 15 \nu \frac{u'^2}{\varepsilon} \quad (2.6)$$

$$\eta = \left(\frac{\nu^3}{\varepsilon} \right)^{(1/4)} . \quad (2.7)$$

Correspondingly, the large-eddy turn-over time is defined by $T = L_{int}/u'$ and the Kolmogorov time as $t_{kol} = 1/\omega'$; the Taylor micro-scale Reynolds number is $Re_\lambda = u' \lambda/\nu$.

3. The initial field

At the moment the initial field of our simulation is prescribed in a way similar to the one proposed by Rogallo (1981). We assume an initial three-dimensional energy spectrum $E(k, t=0)$ of the following form:

$$E(k, t=0) = \frac{3u'}{A} \frac{k^\sigma}{k_p^{\sigma+1}} \exp\left(-\sigma \frac{k}{k_p}\right) , \quad (3.1)$$

where $A = \int_0^\infty k^\sigma \exp(-\sigma k) dk$. k_p sets the ‘‘peak-wavenumber’’ modulus of the prescribed spectrum (the subscript of k_p should not be confused with a ‘‘directional’’ subscript of the wavenumber vector k_i) essentially used for controlling the relationship between Reynolds number and (numerical) Fourier-space sample size while σ is the exponent of the power-law decay (Mansour & Wray (1994)).

The velocity field is assigned with randomly scrambled phases and verifying the continuity constraint, such that its Fourier coefficients read:

$$\hat{u}_i(k) = \alpha e_i^1 + \beta e_i^2 , \quad (3.2)$$

with e_i^1, e_i^2 mutually orthogonal unit vectors in the plane orthogonal to the wave vector k . The complex factors α, β are given by:

$$\begin{aligned} \alpha &= \sqrt{\frac{E(k, t=0)}{4\pi k^2}} \exp(i\theta_1) \cos(\phi) , \\ \beta &= \sqrt{\frac{E(k, t=0)}{4\pi k^2}} \exp(i\theta_2) \sin(\phi) , \end{aligned} \quad (3.3)$$

with θ_1, θ_2, ϕ uniformly distributed pseudo-random numbers on the interval $(0, 2\pi)$ and $i^2 = -1$.

4. The synthetic energy input

Sometimes it is desirable to counteract natural dissipation in order to prevent a rapid decay of the turbulent motion. For this purpose, energy can be injected continuously into the system by defining an appropriate body force coefficient $h(k)$ in wavenumber space. Energy is in general ‘‘pumped’’ into the large scales at a magnitude equal to the initial global energy dissipation such as to allow for a controlled equilibrium flow. Squaring (2.2) and integrating over all wavenumbers, we obtain the equation for the temporal evolution

	case	N	σ	k_p	ν	forcing	$k_{max}\eta$	Re_λ	L_{int}/L_{box}
————	256_a	256	4	13	0.0007	–			
----	256_b	256	4	5	0.0033	✓	2	50	0.08
— · — ·	256_c	256	4	5	0.0016	✓	$\sqrt{2}$	70	0.08

TABLE 1. Parameters of the present simulations: line style, number of Fourier modes N , initial spectral decay coefficient σ , peak wavenumber k_p , viscosity ν ; small-scale resolution $k_{max}\eta$, Taylor Reynolds number Re_λ and integral scale with respect to the computational box L_{int}/L_{box} . The last three values are taken at the “equilibrium” state and are therefore not available in the freely-decaying case 256_a.

of the turbulence intensity:

$$\partial_t q^2 = -\varepsilon + q^2 3 \int_k h(k) dk \quad . \quad (4.1)$$

By normalizing the forcing function $h(k)$ in the following way

$$h(k) = \frac{a(k)}{3 q^2 \int_k a(k) dk} P_{input} \quad , \quad (4.2)$$

we obtain a simple balance for turbulence intensity: $\partial_t q^2 = P_{input} - \varepsilon$. It is seen that P_{input} is the power input into the system; $a(k)$ is a normalized forcing spectrum.

As in all cases, the particular form of the forcing is a matter of choice. In the code of A. Wray, the power input is distributed over a narrow band of wavenumbers around the peak of the initially selected spectrum, viz:

$$a(k) = \begin{cases} 1 & \text{if } k_p - 1 \leq k \leq k_p + 1 \\ 0 & \text{otherwise} \end{cases} \quad . \quad (4.3)$$

The condition $P_{input} = \varepsilon(t=0)$ is imposed. Independently, a numerical “target” resolution $k_{max}\eta$ is reached during the steady state by assigning the corresponding viscosity ν which is obtained from substitution of (2.4) and (2.7) and integrating (3.1) accordingly. The numerical limiting wavenumber as defined in the code is $k_{max} = \sqrt{2}/3 N$ where N is the number of modes in the Fourier expansion $\exp(\pm i k_j x_j) = 0, \dots, \frac{1}{2}N$. Note that the largest numerical wavenumber modulus should actually rather be $\sqrt{3}N/2$.

5. The chosen parameter set

The parameters of our present simulations are shown in table 1; the cases can be further subdivided into freely-decaying and forced simulations.

5.1. Freely-decaying case

In the decaying case (run 256_a) the initial Taylor micro-scale Reynolds number is $Re_\lambda = 180$ with an evolution as shown in figure 1. The resolution is initially marginal while the box is large compared to the integral length scale (cf. figures 3 and 2). The simulation has been run for approximately 420 Kolmogorov time units of the initial field, T_{kol0} , which corresponds to 6.4 initial large-eddy turnover times. This simulation took 6h of wall-clock time on 128 processors of the T3E machine at ZIB, Berlin.

The energy decay is shown in figure 4, following a power-law with a coefficient of roughly -1.4 at later times. The build-up of a realistic values for the velocity derivative

skewness can be deduced from figure 6. The evolution of the energy spectrum from its initially unrealistic shape can be observed in figure 7.

The state of the flow-field at the end of the present simulation with respect to the presence of coherent structures was briefly investigated by flow visualization. Figure 10 shows an isocontour plot of vorticity magnitude $|\omega|$ in a sub-volume of the computational box at an instant that corresponds to $Re_\lambda = 35$. At a threshold of $|\omega| \geq 3\omega'$ one can distinguish structures which are reminiscent of the characteristic ‘worms’ (cf. e.g. Jiménez & Wray (1998)). It is also clear that a higher resolution should be envisaged for the study of such small-scale phenomena (note that $k_{max}\eta \approx 1$ at that time). Jiménez & Wray (1998) use $k_{max}\eta = 1$ during most of the simulations and then increase the resolution to $k_{mak}\eta \geq 2$ shortly before output of the data fields.

5.2. Forced cases

Two simulations with large-scale forcing were conducted: a low-Reynolds number case and one at medium Reynolds-number (named 256_b and 256_c respectively); the settling towards the respective ‘asymptotic’ values of Re_λ can be observed in figure 1. The small-scale resolution is excellent in both cases (figure 2 and flow visualizations below) while the large-scale sample remains also very large (figure 3). Figure 5 demonstrates that the turbulent kinetic energy tends towards a constant value at the end of both runs after initially starting off with a zero slope (due to the use of $P_{input} = \varepsilon(0)$) and then decaying (due to an increase in ε itself). The velocity derivative skewness takes on values similar to the freely-decaying case (figure 6).

The spectra shown in figures 8 and 9 are rather rapidly converging towards a seemingly stationary shape, over a time of $t/t_{kol0} \sim \mathcal{O}(10)$.

Finally, the visualization of high-vorticity structures (figures 11 and 12) underlines again the quality of the resolution.

6. Further procedure

We will conduct a forced run over sufficiently large time to obtain converged low-order statistics which can be compared to those published in the literature. Having confidence in the parameter range, we will then proceed to produce three types of time-series of instantaneous fields: (i) while further forcing the flow; (ii) just after switching off the energy input; (iii) at a somewhat later stage of the free decay (‘somewhat’ needs to be further specified).

We will perform these simulations at resolutions of 256 and 512 spectral modes (1024 should also be possible technically), also carrying out some reduced tests of grid refinement.

The small-scale resolution will be kept similar to the one used in cases 256_b and 256_c. The peak of the energy spectrum can be safely moved further towards the small wavenumbers so that a higher Reynolds number should also be possible. We target for $Re_\lambda \approx 140$ when using 512 modes.

7. Acknowledgements

The code for the present simulation was kindly provided by A. Wray of NASA Ames. The computational resources of ZIB, Berlin, are gratefully acknowledged.

REFERENCES

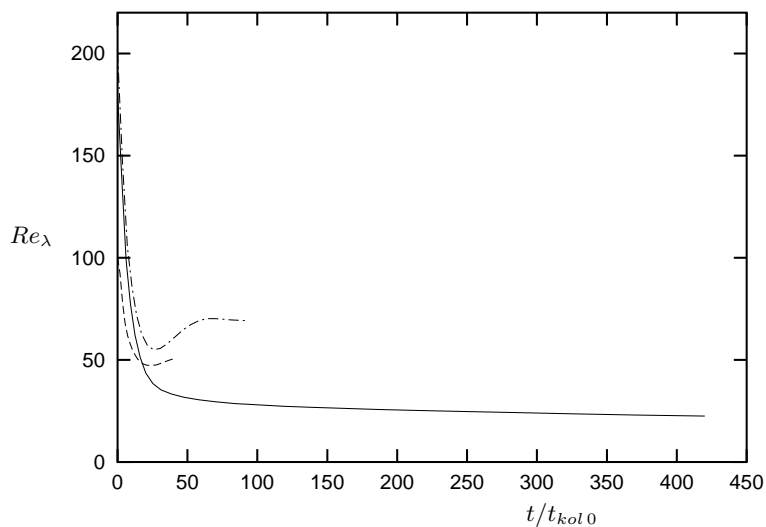


FIGURE 1. Evolution of the Taylor microscale Reynolds number during the course of the present simulations. Line types are as in table 1.

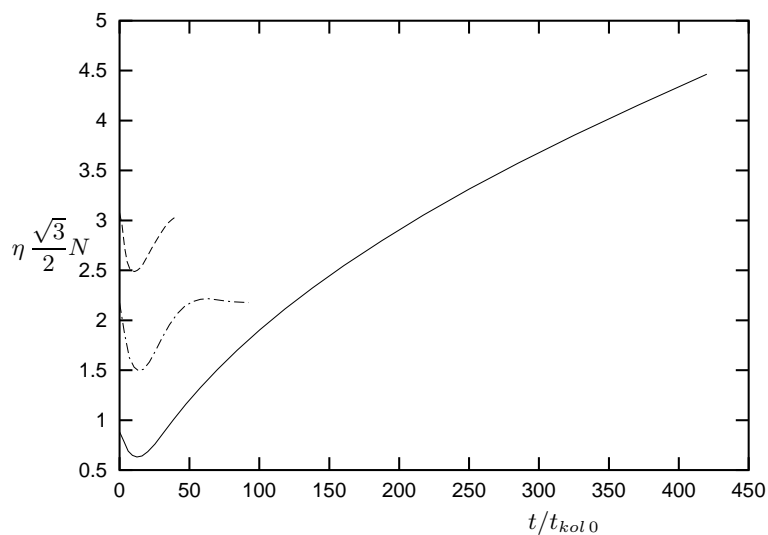


FIGURE 2. Evolution of the small-scale resolution parameter.

JIMÉNEZ, J. & WRAY, A. 1998 On the characteristics of vortex filaments in isotropic turbulence. *J. Fluid Mech.* **373**, 255–282.

KLEIN, R. 1998 Kleinskalige Instabilitäten als Bausteine der turbulenten Energiekaskade. DFG-Antrag auf Gewährung einer Sachbeihilfe, Projekt KL 611/10 (in German).

MANSOUR, N. & WRAY, A. 1994 Decay of isotropic turbulence at low Reynolds number. *Phys. Fluids* **6** (2).

ROGALLO, R. 1981 Numerical experiments in homogeneous turbulence. *Tech. Rep.* TM 81315. NASA.

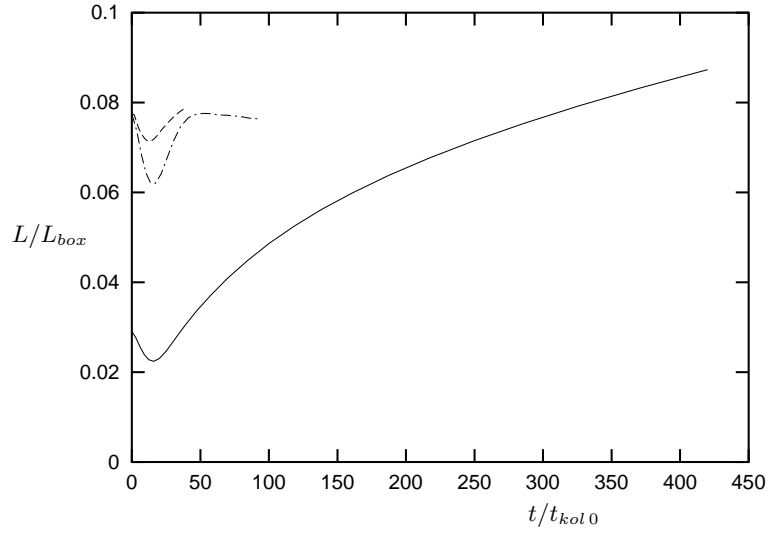


FIGURE 3. Evolution of the relative box size

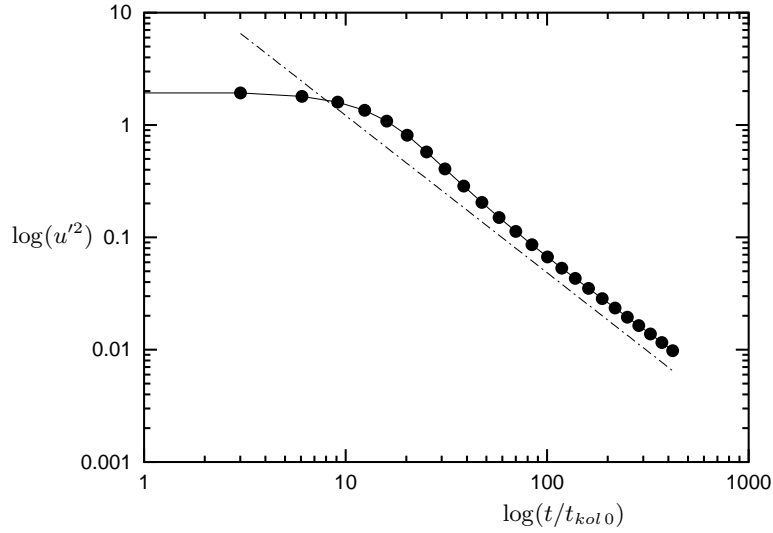


FIGURE 4. Temporal decay of the turbulent kinetic energy of the flow in case 256_a. The straight reference line has a negative slope of 1.4.

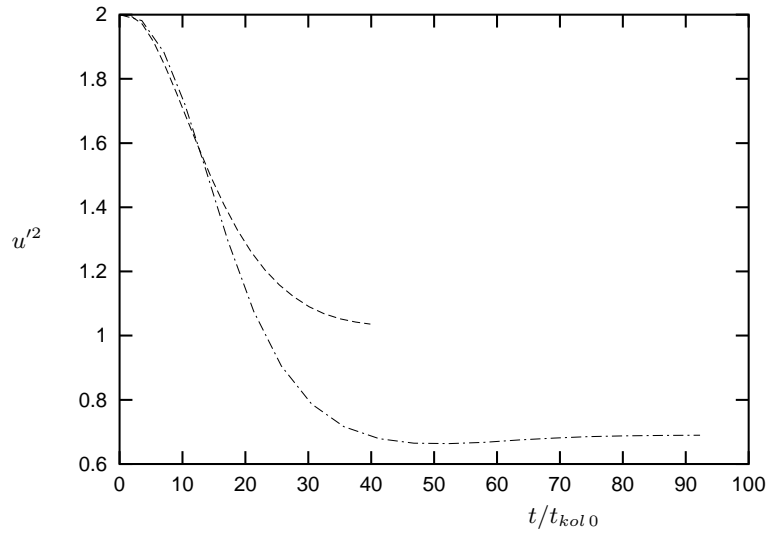


FIGURE 5. Temporal evolution of the turbulent kinetic energy of the flow in the two forced cases 256_b and 256_c.

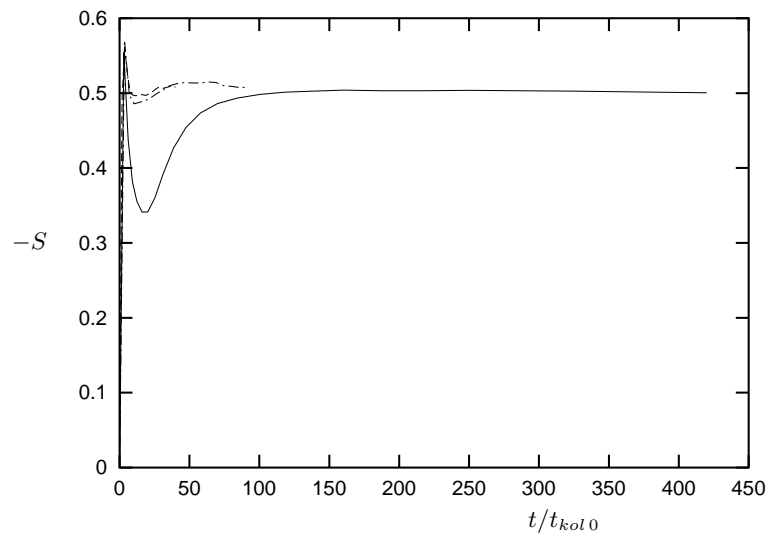


FIGURE 6. Evolution of the velocity derivative skewness.

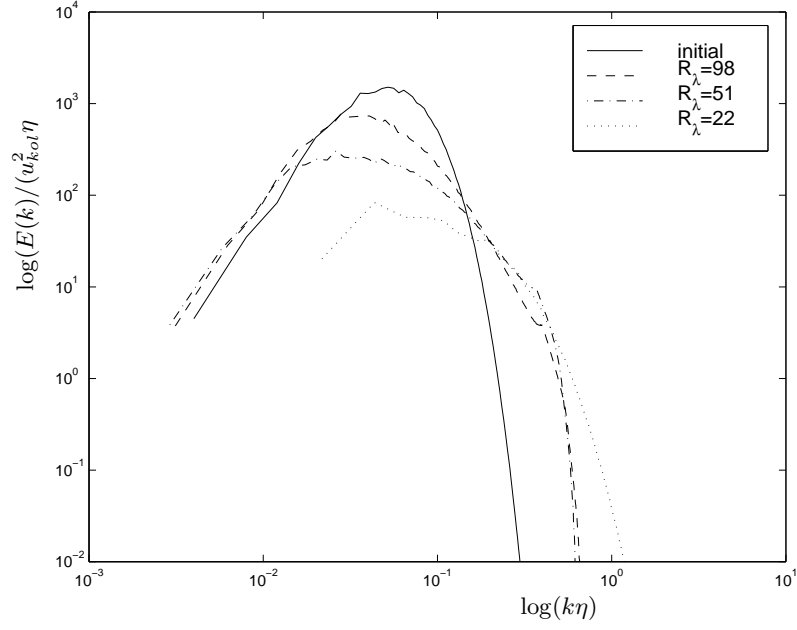


FIGURE 7. Evolution of energy spectrum at various stages of the simulation 256_a.

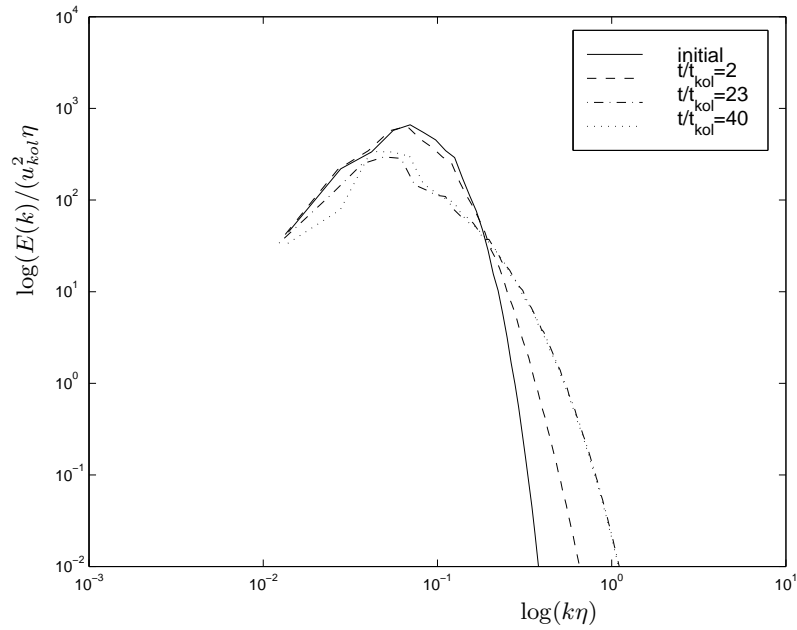


FIGURE 8. Evolution of energy spectrum at various stages of the simulation 256_b.

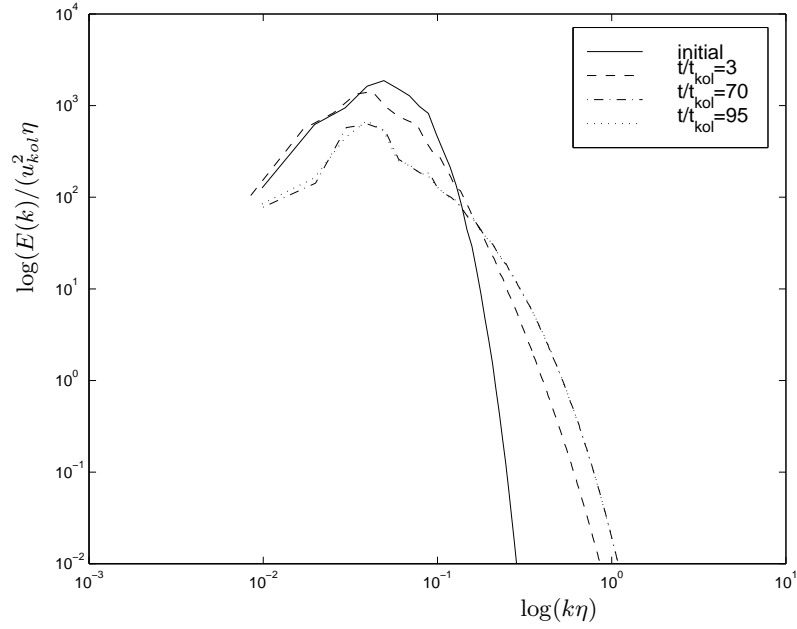


FIGURE 9. Evolution of energy spectrum at various stages of the simulation 256_c.

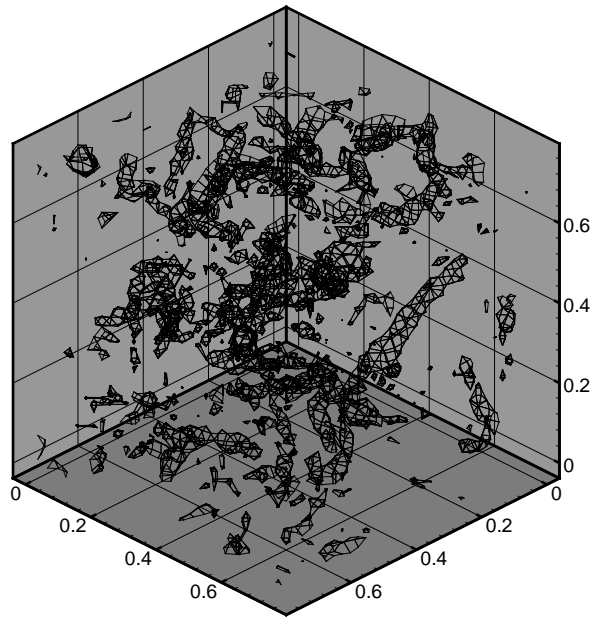


FIGURE 10. Isocontours of vorticity magnitude $|\omega|$ at a level of three times the current r.m.s. value, taken at $t/t_{k,col} = 31$ when $R_\lambda = 35$. The linear dimension of the selected sub-volume measures roughly 200η .

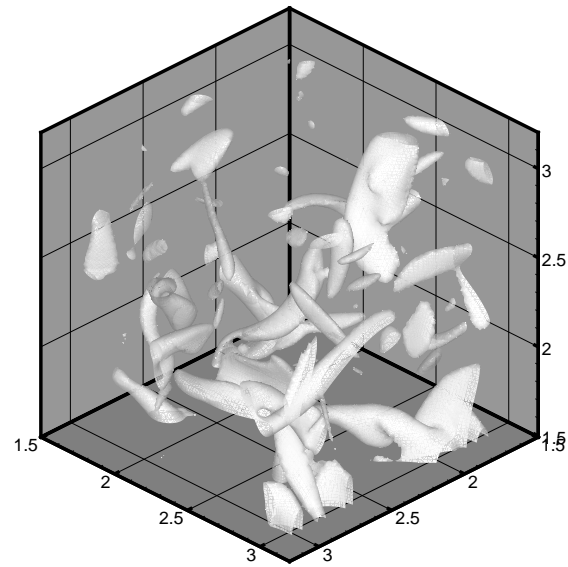


FIGURE 11. Isocontours of vorticity magnitude $|\omega| = 3\omega'$, taken at the end of case 256_b ($R_\lambda \approx 50$). The linear dimension of the selected sub-volume measures roughly 110η .

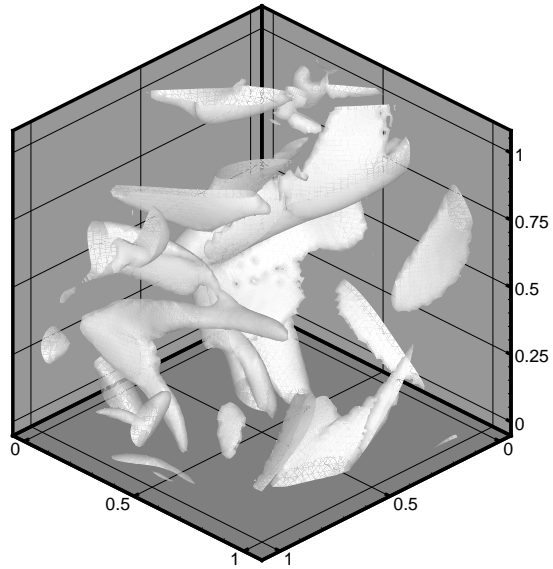


FIGURE 12. Isocontours of vorticity magnitude $|\omega| = 3\omega'$, taken at the end of case 256_c ($R_\lambda \approx 70$). The linear dimension of the selected sub-volume measures roughly 110η .